

## Contacting State on Imaginary Rack of Crossed Helical Gears

Emma TAMUTA\*<sup>1</sup>, Ryozo NEMOTO\*<sup>2</sup>, Hirotaka TOMITA\*<sup>3</sup>,  
Eiichirou TANAKA\*<sup>4</sup> and Hideo TAKAHASHI\*<sup>5</sup>

- \*1, 2, 3 Tokyo Metropolitan College Industry Technology  
8-17-1 Minamisenju, Arakawa-ku, Tokyo 116-0003, JAPAN  
ema@acp.metro-cit.ac.jp, nemotor@acp.metro-cit.ac.jp, tomita@acp.metro-cit.ac.jp
- \*4 Shibaura Institute of Technology  
307 Fukasaku, Minuma-ku, Saitama-shi 337-8570, JAPAN  
tanakae@shibaura-it.ac.jp
- \*5 Kisarazu National College of Technology  
2-11-1 Kiyomidai-Higashi, Kisarazu, Chiba 292-0041, JAPAN  
takahasi@m.kisarazu.ac.jp

### Abstract

The parts of crossed helical gears have no difference as those of helical gears with parallel axes, because crossed helical gear is able to be manufactured in the same way as single helical gear, using the same cutting tool. Because there is no difference between a crossed helical gear and a helical gear, that is, several advantages of mounting the gear in a gear box exist. The close accuracy in center distance, shaft angle and axial position does not affect the conjugate action of crossed helical gears. As mentioned above, crossed helical gears have several advantages [1], [2] of the application. However, crossed helical gears have also disadvantages. One is that contact stress between the tooth surfaces of crossed helical gears becomes comparatively high. Another is that sliding velocity on tooth surfaces becomes higher than for other kinds of gears [3]. The purpose of this paper is exactly to investigate the contact stress state on the tooth surfaces of crossed helical gears.

**Keywords:** machine element, gears, crossed helical gears, contact stress, contact ellipse

### 1 Introduction

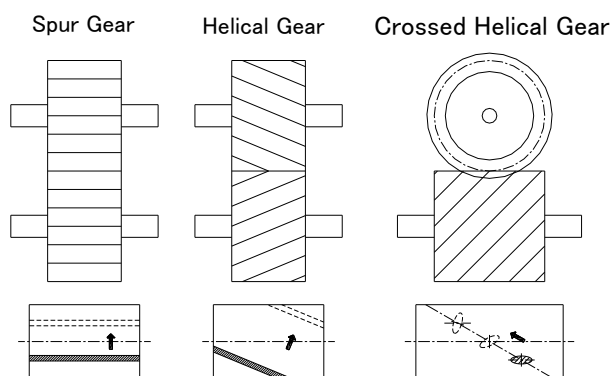


Fig. 1 Contacting state on imaginary rack

Figure 1 shows the contacting state on imaginary rack of 3 kinds of gearing, respectively spur, helical and crossed helical. In the case of spur gearing, contact between tooth, theoretically takes place at a line or two lines. The contact line becomes a rectangle due to deformation under loading. In the case of helical gearing, contact between tooth surfaces occurs along a diagonal line or becomes parallelogram. In the case of crossed helical gearing, the contact between teeth has only point contact instead of contact across a face width and contact point becomes an ellipse due to elastic deformation under loading.

Figure 2 shows view of crossed helical gears. Crossed helical gears are used to transmit motion and power. Shafts in crossed helical gears are nonparallel. Crossed helical gears have several advantages. One is that they are able to be manufactured by any machine, especially the hobbing machine. Another is that slight changes in shaft angle and center distance do not affect the conjugate action. In spite of these, crossed helical gears have not only advantages but also have disadvantages. One is that the contact stress on tooth surface is relatively high, because the contact of gear teeth geometrically takes place at a point. Another is that the relative slide between the tooth surfaces is notably large.



Fig. 2 View of crossed helical gears

In a crossed helical gear pair, **Fig. 3** shows the relationship between two base cylinders of gears and a line of action. Gear 1 is the driver gear. Gear 2 is the follower gear. In **Fig. 3**  $C$  is the contact point. This contact point  $C$  is moving on the line of action  $QH$ .  $QH$  means the common internal tangent to the two base cylinders. In this figure the shaft angle  $\delta$  is the angle between the two axes of base cylinders.  $\rho_1$  and  $\rho_2$  are radii of curvature of tooth surfaces respectively. Line  $AA$  is the contact line between the imaginary rack and the tooth surface of gear 1. Line  $BB$  is the contact line between the imaginary rack and the tooth surface of gear 2. The total length of action line  $QH$  is constant.  $QH$  was represented as “ $w$ ” by equation (1).

$$w = \frac{a - r_{b1} \cdot \cos \alpha_{t1} - r_{b2} \cdot \cos \alpha_{t2}}{\sin \alpha_n} \quad (1)$$

$$= \frac{r_{b1} \cdot \tan \alpha_{t1}}{\cos \beta_{b1}} + \frac{r_{b2} \cdot \tan \alpha_{t2}}{\cos \beta_{b2}}$$

$a$ [mm]: Center distance  
 $r_{b1}$ [mm]: Radius of base cylinder of gear 1  
 $r_{b2}$ [mm]: Radius of base cylinder of gear 2  
 $\alpha_n$  [deg]: Normal pressure angle  
 $\alpha_{t1}$  [deg]: Transverse pressure angle  
 $\alpha_{t2}$ [deg]: Radius of base cylinder of gear 2  
 $\beta_{b1}$ [deg]: Helix angle on base cylinder of gear 1  
 $\beta_{b2}$ [deg]: Helix angle on base cylinder of gear 2

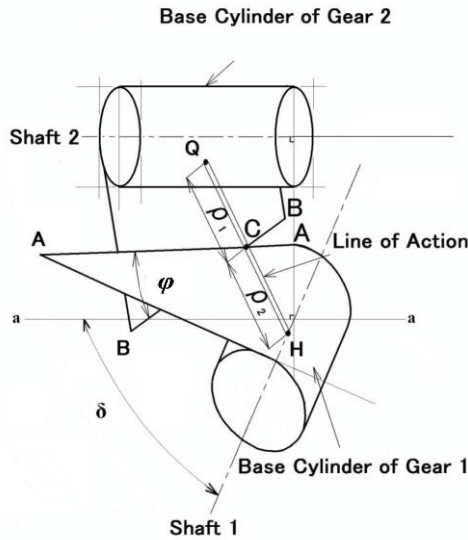


**Fig. 3** Relationship between two base cylinders and an action line

At pitch point  $\rho_1$  and  $\rho_2$  are represented by equations (2) and (3), respectively.

$$\rho_{1p} = \frac{r_{w1} \cdot \sin \alpha_n}{\cos^2 \beta_{b1}} = \frac{d_{w1} \cdot \sin \alpha_n}{2 \cos^2 \beta_{b1}} \quad (2)$$

$$\rho_{2p} = \frac{r_{w2} \cdot \sin \alpha_n}{\cos^2 \beta_{b2}} = \frac{d_{w2} \cdot \sin \alpha_n}{2 \cos^2 \beta_{b2}} \quad (3)$$

$r_{w1}$ [mm]: Radius of pitch cylinder of gear 1  
 $r_{w2}$ [mm]: Radius of pitch cylinder of gear 2  
 $d_{w1}$  [mm]: Diameter of working pitch cylinder of gear 1  
 $d_{w2}$  [mm]: Diameter of working pitch cylinder of gear 2

The radii of equivalent cylinders are represented as the following equations (4), (5), (6) and (7).

$$\rho_{1\max} = \rho_{1p} + e_{n1\max} = \frac{\sqrt{r_{a1}^2 - r_{b1}^2}}{\cos \beta_{b1}} \quad (4)$$

$$\rho_{2\max} = \rho_{2p} + e_{n2\max} = \frac{\sqrt{r_{a2}^2 - r_{b2}^2}}{\cos \beta_{b2}} \quad (5)$$

$$\rho_{1\min} = w - \rho_{2\max} \quad (6)$$

$$\rho_{2\min} = w - \rho_{1\max} \quad (7)$$

$r_{a1}$ [mm]: Radius of tip cylinder of gear 1  
 $r_{a2}$  [mm]: Radius of tip cylinder of gear 2

**Figure 4** shows the engagement of the imaginary rack inserted between the tooth surfaces of gears 1 and 2. In **Fig. 4** line  $AA$  is the contact line between the imaginary rack and the tooth surface of gear 1. Line  $BB$  is the contact line between the imaginary rack and the tooth surface of gear 2.

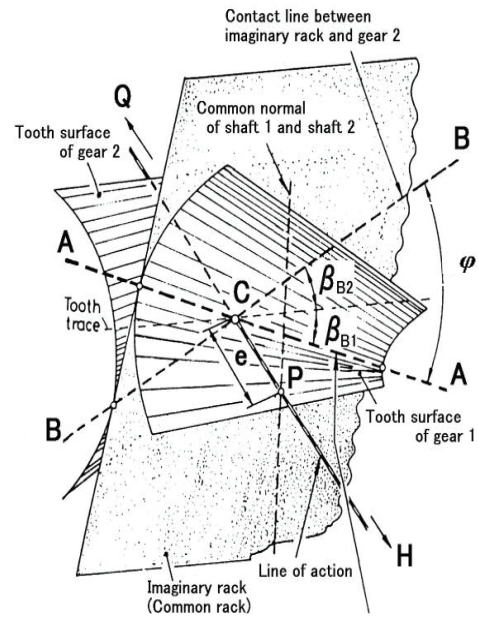


**Fig. 4** Engagement of crossed helical gear

Engagement of tooth surfaces of crossed helical gears can be replaced by the contact of two equivalent

cylinders with the shaft angle  $\varphi$  as shown in **Fig. 5**. Equivalent cylinder 1 and 2 are geometrically contacting at point  $C$ . According to loading, this contacting point  $C$  changes to a contact ellipse due to elastic deformation of tooth surfaces. When two cylinders of same diameter  $d$  with skew axes are pressed together with a normal pressure  $P_N$ , a contact ellipse is obtained. **Figure 6** shows the contact ellipse on the imaginary rack of crossed helical gears [7], [8].

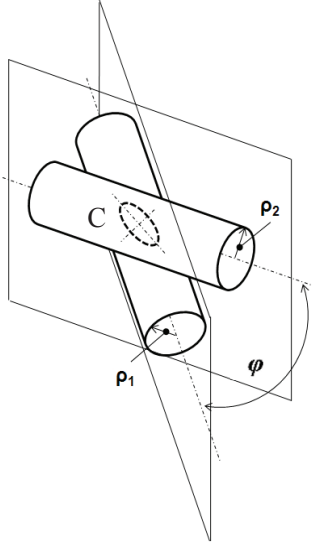


**Fig. 5 Two equivalent cylinders of crossed helical gears**

The shaft angle  $\varphi$  between two equivalent cylinders is represented [3] by equations (8) and (9).

$$\varphi = \beta_{B1} + \beta_{B2} \quad (8)$$

$$\sin \varphi = \frac{\sin \alpha_n \cdot \sin \delta}{\cos \beta_{b1} \cdot \cos \beta_{b2}} \quad (9)$$

$\beta_{B1}$  [deg]: Angle between contact line  $AA$  and tooth trace

$\beta_{B2}$  [deg]: Angle between contact line  $BB$  and tooth trace

$\delta$  [deg]: Shaft angle of crossed helical gear

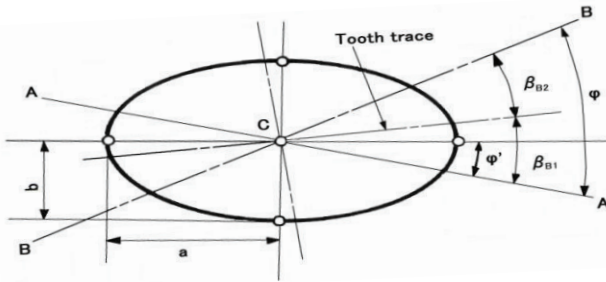


**Fig. 6 Contact ellipse on imaginary rack of crossed helical gears**

In the general case [4], [5], [6], the maximum contact stress  $P_{Hmax}$  is represented by using Hertzian auxiliary.

$$P_{Hmax} = \frac{3}{2} \cdot \frac{P_N}{\pi \cdot a \cdot b} \quad (10)$$

$a$  [mm]: A half of major axis of an ellipse

$b$  [mm]: A half of minor axis of an ellipse

Two auxiliary coefficients  $\xi$  and  $\eta$  are derived by the following equations (11) and (12).

$$a^3 = 3 \cdot \xi^3 \cdot \frac{(1-\nu^2) \cdot P_N}{E \cdot \sum 1/\rho} \quad (11)$$

$$b^3 = 3 \cdot \eta^3 \cdot \frac{(1-\nu^3) \cdot P_N}{E \cdot \sum 1/\rho} \quad (12)$$

$\nu$  [-]: Poisson's ratio

$E$  [MPa]: Young's modulus

$\xi$  and  $\eta$  are represented by using complete elliptic integral of second kind  $E(k)$  as following equations (13) and (14).

$$\xi^3 = \frac{2}{\pi} \cdot \frac{E(k)}{1-k^2} \quad (13)$$

$$\eta^3 = (1-k^2)^{3/2} \cdot \frac{2}{\pi} \cdot \frac{E(k)}{1-k^2} = (1-k^2)^{3/2} \cdot \xi^3 \quad (14)$$

$k$  [-]: Eccentricity of an ellipse  $k = \frac{\sqrt{a^2 - b^2}}{a}$

In the general case, the following equation (15) is geometrically formed [4], [5].

$$\left( \frac{1}{\rho_{21}} - \frac{1}{\rho_{22}} \right) \sin 2(\varphi - \varphi') = \left( \frac{1}{\rho_{11}} - \frac{1}{\rho_{12}} \right) \sin 2\varphi' \quad (15)$$

$\rho_{11}, \rho_{12}$  [mm]: Principal radii of curvature at the point of contact for the body 1

$\rho_{21}, \rho_{22}$  [mm]: Principal radii of curvature at the point of contact for the body 2

Furthermore, the radii of curvatures ( $\rho_{12}$  and  $\rho_{22}$ ) along the generating lined become infinity. As showing in **Fig. 5**, the above-mentioned is equivalent to the contact two cylinders with skew axes.

In the case of crossed helical gears, the following equation (16) was represented by one of the present authors [9], [10], [11].

$$\tan \varphi' = \frac{F \cdot \sin 2\varphi}{1 + F \cdot \cos 2\varphi} \quad (16)$$

The variable  $F$  in equation (16) is the ratio of radius of equivalent cylinders.  $F$  equals to  $\rho_1$  divided by  $\rho_2$ .

The value of angle  $\varphi$  is independent on the displacement of contact point. However the value of angle  $\varphi'$  is dependent on the displacement of contact point.

## 2 Experiment

Figure 7 shows the experimental apparatus. This simplified experimental test was carried out to prove equation (16). The prescale film was used to measure pressure. The prescale film was inserted between the upper cylinder and the lower one in the Fig. 7. Two cylinders were made from the same materials. Acrylic resin was used as test material. Poisson's ratio  $\nu$  equals 0.385. Young's modulus  $E$  equals  $4.49 \times 10^3$  [MPa].

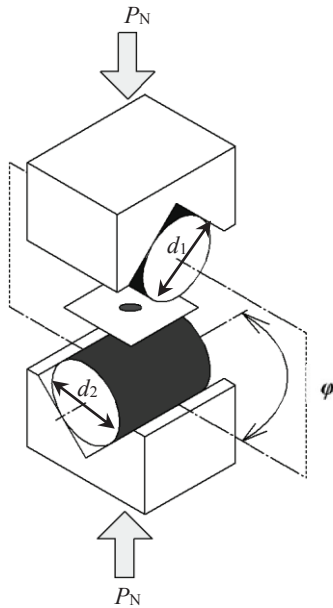


Fig. 7 Experimental apparatus for two cylinders

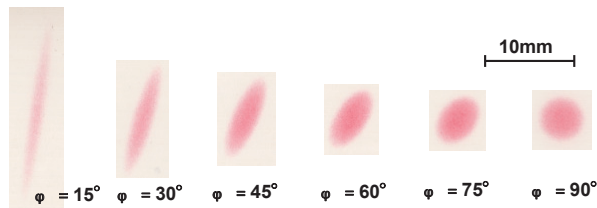


Fig. 8 Measured contact ellipses

Table 1 Inclination angle

$\varphi$ [deg]	$\varphi'$ [deg] (calc.)	$\varphi'$ [deg] (exp.)
15	7.5	6.5
30	15.0	17.0
45	22.5	22.0
60	30.0	33.0
75	37.5	38.0
90	45.0	45.0

Test experimental apparatus was loaded by oil pressure. These experiments were carried out by pressing an upper cylinder upon a lower cylinder. Upper cylinder and lower cylinder have same diameter. They equal to 67.5[mm]. We measured the inclination angle of the ellipse by protractor.

Measured contact ellipses between two cylinders by changing shaft angle  $\varphi$  in the case of  $P_N = 1472$ [N] are shown in Fig. 8. Table 1 shows the experimental and calculated values of inclination angle. The experimental values were determined by reading the patterns of ellipse in Fig. 8. The calculated values were resulted by using equation (16). As shown in Table 1, experimental results are in good agreement with theoretical calculation.

## 3 Contact stress state on the tooth surface

Figures 9, 10, 11 and 12 show the progress of engagement on imaginary rack about crossed helical gear. A pair of crossed helical gears has a shaft angle  $\delta$  of  $90^\circ$  and a center distance  $a$  of 80.61[mm]. The driver and follower gears are identical. These figures show in the case of normal module  $m_n = 3.0$  and tooth number  $z = 19$ .

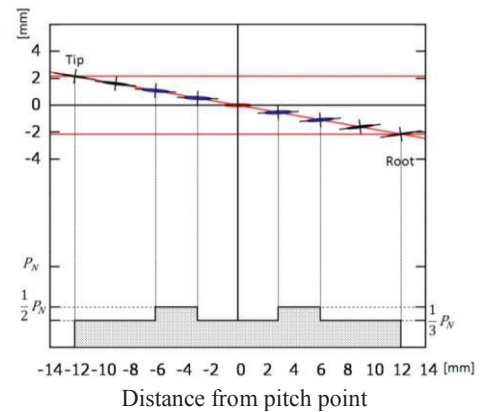
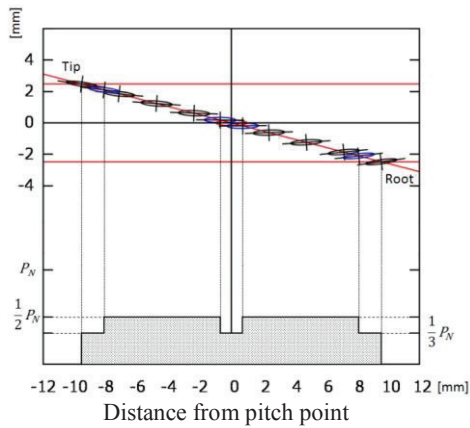
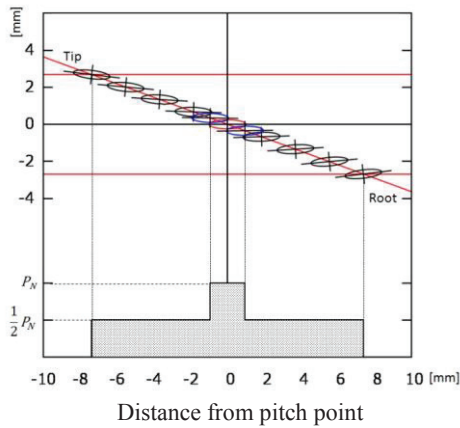


Fig. 9 Contact stress state on tooth  $\alpha_n=10$ [deg],  $m_n=3.0$



**Fig. 10 Contact stress state on tooth**  
 $\alpha_n=14.5[\text{deg}]$ ,  $m_n=3.0$



**Fig. 11 Contact stress state on tooth**  
 $\alpha_n=20[\text{deg}]$ ,  $m_n=3.0$

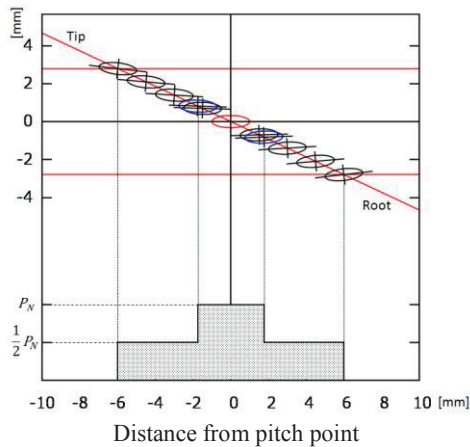


**Fig. 12 Contact stress state on tooth**  
 $\alpha_n=25[\text{deg}]$ ,  $m_n=3.0$

Concerning driver gear, the direction of progress is from extreme right to extreme left. A center ellipse in these figures was calculated at pitch point. According to the progress of engagement, contact ellipse on tooth surface rotates clockwise.

## 4 Conclusions

The following conclusions were drawn from the contacting state on imaginary rack.

- (1) The inclination of contact ellipse from the result of the simplified experiment is good agreement with one obtained from theoretical calculation.
- (2) Details of variations of the contact ellipse on tooth surface of crossed helical gears were observed. According to the progress of engagement, contact ellipse on tooth surface rotates clockwise.

## References

- [1] Schiebel, A., Zahnraeder, Zweter Teil, (1923), Verlag Springer, Berline.
- [2] Buckingham, E., Analytical mechanics of gears, (1949), McGraw Hill, New York & London.
- [3] Niemann, G., and Winter, H., Mashinenelemente Bd. 3, (1983), Springer Verlag, pp. 1-19.
- [4] Love, A.E.H., (1944), A Treatise on the Mathematical Theory of Elasticity, Dover pp. 192-198.
- [5] Hastings, C., Approximations for Digital Computers, (1955), Princeton Univ. Press, 170.
- [6] Hertz, H., Journal fuer die reine und angewandte Mathematik, 92 (1882), 156.
- [7] Brewe, D., and Hamrock, B., Transactions of ASME, Journal of Lubrication Technology, Oct. (1977), 485.
- [8] Grekousis, R., and Michailidis, (1981), "Naeherungsgleichungen zur Nach- und Entwurfsrechnung der Punktberuehrung nach Hertz", Konstruktion, Th., 33 H.4,S. Springer Verlag, pp. 135-139.
- [9] Nemoto, R., Naruse, Ch., Haizuka, Sh., and Nakagawa, T., (1995), "Influence of Surface Treatment, Tooth Form and Lubricating oil on Load Carrying Characteristics of Crossed Helical Gears", JSME International Journal. 38-1, pp.94-105.
- [10] Nemoto, R., Naruse, Ch., and Haizuka, Sh., (1996), "Le sollecitazioni di contatto in ingranaggi sghembi", ORGANI DI TRASMISSIONE, comandi e azionamenti, tecniche nuove, Milano, Numero 8 settembre, pp. 116-119.
- [11] R.Nemoto, E.Tamura, H.Tomita, E.Tanaka and H.Takahashi., (2013), "Improvement of load-carrying Capacity by adopting the low pressure angle (In the case of crossed helical gears)". VDI-Berichte 2199.2, ISBN978-3-18-092199-0, pp.1267-1278.

Received on November 30, 2013

Accepted on February 4, 2014